

## KINEMATIC STRUCTURE OF THE TRANSITION-ZONE DOWNDRAFT IN THE 10-11 JUNE 1985 SQUALL LINE OBSERVED OVER KANSAS AND OKLAHOMA

Michael I. Biggerstaff and Robert A. Houze, Jr.

Department of Atmospheric Sciences  
University of Washington

### 1. INTRODUCTION

As part of the Oklahoma-Kansas Preliminary Regional Experiment for Stormscale Operational Research Meteorology—Central Phase (PRE-STORM) (see Cuning 1986) two 5-cm wavelength Doppler radars operated by the National Center for Atmospheric Research (NCAR) were deployed just west of Wichita, Kansas, on a 60-km NNW-SSE baseline. Coordinated sequences of scans at elevation angles of  $0.2^\circ$  to  $58^\circ$  were collected during May-June 1985 to study the structure and evolution of Mesoscale Convective Systems (MCSs).

During the passage of MCSs, data collection at the two Doppler sites was virtually continuous. One MCS that was particularly well sampled occurred during 10-11 June 1985 and consisted of a squall line with trailing-stratiform precipitation (Rutledge et al. 1988; Johnson and Hamilton 1988; Houze et al. 1989). Recently, Biggerstaff and Houze (1991) analyzed the relationship between the storm relative flow and the trailing-stratiform precipitation region in this storm and found a region of deep subsidence immediately behind the convective line in the "transition zone", which is the zone of lower reflectivity behind the intense convective line and head of the zone of heaviest stratiform rain (Fig. 1). That analysis, however, was too coarse to resolve the character of the deep subsidence and could not address how the subsidence may have developed.

In this paper, we use a series of high-resolution dual-Doppler analyses from the NCAR Doppler radars taken during the passage of the 10-11 June 1985 squall-line system to investigate further the average temporal and spatial structure of the deep subsidence found in the transition zone. We show that the average structure can be explained by the storm relative movement of transient vertical drafts associated with dissipating convective cells toward the rear of the convective region.

### 2. DATA AND METHOD OF ANALYSIS

Simultaneous data from the two NCAR Doppler radars for scans beginning at 0131, 0139, 0209, 0220, 0345, 0414, and 0510 UTC were considered. All scans except for 0131, 0220, and 0510 were taken by sweeping azimuthally over a  $360^\circ$  conical surface. This procedure provided data for analysis on both sides (hereafter called the east and west lobes) of the NNW-SSE baseline for several scan times. A series of eleven separate dual-Doppler analyses between the leading line and the back edge of the trailing-stratiform region were constructed. The horizontal wind and radar-reflectivity data from each of the eleven dual-Doppler analyses were then combined into a coordinate framework attached to the moving storm by assuming a storm velocity of  $14 \text{ m s}^{-1}$  from  $300^\circ$  (which is representative of the northern part of the squall-line system where the NCAR Doppler radars were deployed). The grid has 3-km horizontal spacing and 0.5-km vertical spacing. The basic kinematic structure of the composite storm was not very sensitive to the assumed storm speed. All data falling into each  $3 \text{ km} \times 3 \text{ km} \times 0.5 \text{ km}$  grid box were averaged to

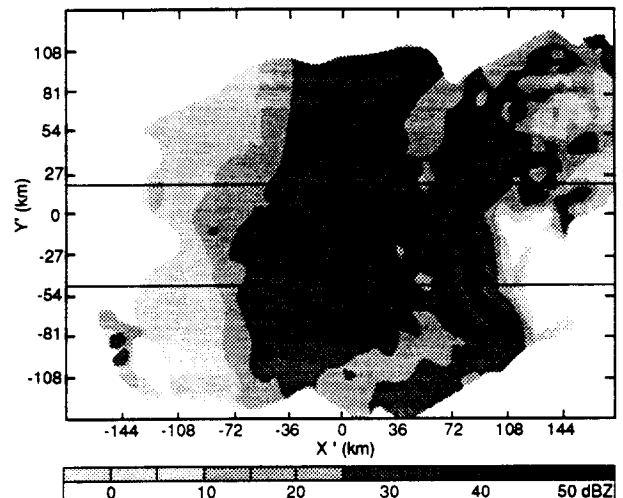


Fig. 1 Composite radar reflectivity in dBZ at 1.9 km above mean sea level. The two horizontal lines enclose the region used in the along-line average shown in Figure 2.

determine the most representative value for that grid volume. Radar reflectivity was converted from log to linear before averaging. Grid boxes with just one estimate were eliminated from the data set. The averages were edited to remove obvious discrepancies which could be traced back to sampling problems. Less than 1% of the data was affected by these two quality checks. The reflectivity data were filtered using a 1-2-1 filter to remove wavelengths less than 6 km. The horizontal wind components were filtered to remove wavelengths less than 18 km after which divergence was calculated and the anelastic continuity equation integrated to obtain the vertical velocity. A boundary condition of  $W_0$  proportional to  $D_{\text{top}}$ , where  $W_0$  is the echo-top vertical velocity and  $D_{\text{top}}$  is the uppermost divergence measurement, was used to initiate the downward vertical integration. To compensate for uncertainties in the horizontal winds, the divergence was then adjusted by setting a second boundary condition ( $W=0$ ) at the surface. Since Doppler data did not extend to the surface, an "influence height" of 2 km was selected to determine the fraction of vertical mass flux at the lowest data level that was to be redistributed with height in each grid column. The adjusted divergence field was then integrated to obtain the adjusted vertical velocity field. The differences in the adjusted and unadjusted vertical velocities were small.

### 3. COMPOSITE STORM STRUCTURE

The composite Doppler-radar data analysis covered a  $360 \text{ km} \times 270 \text{ km}$  area which encompassed the entire breadth of the northern portion of the storm system. The most intense precipitation was associated with the 40-km wide convective band (Fig. 1). Farther back, in the trailing-stratiform region, there was a secondary maximum in

precipitation. The 35-km wide transition zone, characterized by a mid-to-low altitude reflectivity trough, lay between the rear of the convective line and the front of the secondary precipitation maximum.

To illustrate the relationship between deep subsidence and the reflectivity trough found in the transition zone, an along-line average vertical cross section (Fig. 2) was constructed for the most two-dimensional portion of the squall-line system. This region also corresponded closely to the domain of highest resolution and greatest data coverage in the composite analysis. However, because of the limited extent of the individual dual-Doppler analyses (each about 120 km X 120 km), the convective line was sampled at an earlier time than the stratiform region. While this limitation does not affect the results presented here, it is likely that as the stratiform region developed, the convective region sloped more toward the rear of the storm than indicated in the current composite analysis.

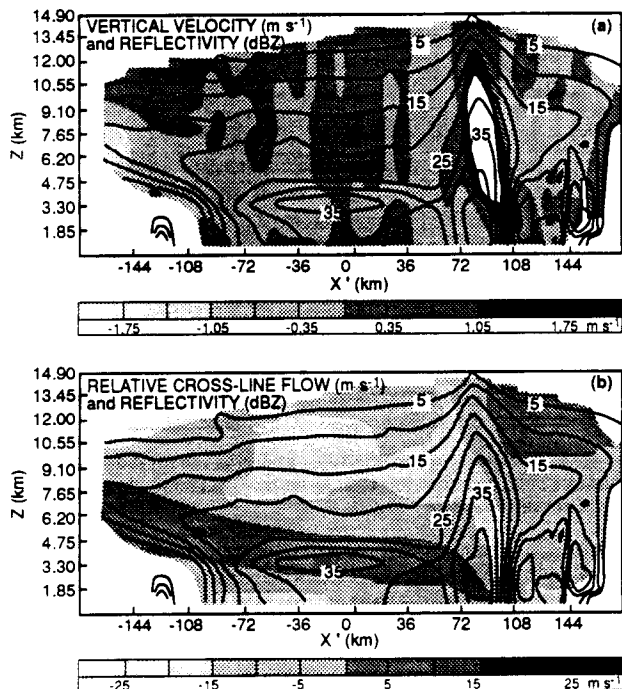


Fig. 2 Mean vertical cross section showing (a) vertical motion in  $m s^{-1}$  according to the gray shading and reflectivity contoured every 5 dB starting at 5 dBZ and (b) storm relative flow in the  $X'$  direction in  $m s^{-1}$  according to the gray shading and reflectivity contoured every 5 dBZ starting at 5 dBZ.

The along-line average composite structure of the observed squall line resembles the time-averaged structure reported in Fovell and Ogura (1988) for a numerical simulation of a similar storm system (Fig. 3). Both the observed and simulated storms exhibited average vertical motions near the convective region that consisted of a mean updraft ahead of the peak reflectivity at low levels and coincident with the peak reflectivity aloft, and three regions of subsidence.

In the observed storm (Fig. 2), a low-level downdraft was found in the convective region in association with the strongest radar reflectivity. It was likely the result of precipitation drag and evaporative cooling. Ahead of the convective region, in the forward anvil, broad subsidence was observed from upper to lower levels and may have been responsible for the pre-squall mesolow reported in Biggerstaff and Houze (1991). Deep subsidence was also found immediately to the rear of the convective region in the transition zone, with the strongest downward motion observed above the reflectivity trough.

Each of three mean downdrafts were observed to some degree in the time-averaged fields of the numerical

simulation (Fig. 3). In particular, the model found, on average, deep subsidence behind the convective line in association with a mid-to-low level reflectivity trough. The time-averaged thermodynamic structure from the simulation suggests that this mean downdraft was positively buoyant.

Thermodynamic retrievals performed on the radar composite data also indicate that the transition-zone downdraft was positively buoyant (Sun et al. 1991). The transition-zone downdraft was not only associated with rear-to-front relative flow near the convective region, but extended upward well into the layer of strong front-to-rear relative flow at mid-to-upper levels just behind the convective line (Fig. 2b). Since the horizontal relative flow was stronger than the vertical motion, the flow must have continued toward the rear of the storm at the same time that it was dynamically forced to descend through the transition zone. The strong mesoscale updraft found in the leading portion of the secondary band may have been aided by the positively buoyant air returning to its equilibrium height as it flowed away from the upper-level dynamic forcing associated with the convective- and transition-zone regions.

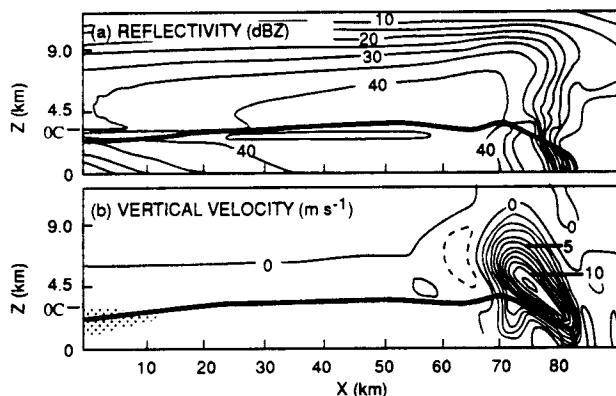


Fig. 3 Time-averaged vertical cross sections from the numerical simulation of Fovell and Ogura (1988) showing (a) radar reflectivity contoured every 5 dBZ starting at 5 dBZ and (b) vertical velocity contoured every 1  $m s^{-1}$  with positive (negative) values solid (dashed).

It is possible that only the upper-level portion of the transition-zone downdraft may have been positively buoyant. An average vertical velocity profile over the transition zone reveals that the subsidence had two well-separated speed maxima (Fig. 4a). Below 5 km, both the transition zone and the secondary band exhibited similar mean vertical motions with a maximum downward motion near the melting level (Fig. 4a). Above 5 km, however, the mean profiles of vertical motion were very different with the secondary band showing weak ascent and the transition zone showing marked subsidence with a peak near 10 km. The double peak in the transition-zone downdraft suggests that two distinctly different processes may have produced the subsidence. Since it is likely that melting and evaporation may have affected the lower portion of the transition zone, that part of the subsidence may have been negatively buoyant.

The divergence profile over the transition zone and secondary band regions also differs most near storm top (Fig. 4b). In the transition zone, the strongest convergence was found at upper levels near 12 km. Over the secondary band, the only significant convergence was found just above the melting level. The strong upper-level convergence in the transition zone is similar to that reported in earlier studies of the convective region of other squall-line systems in which upper-level downdrafts were observed in the convective region in association with strong upper-level convergence created by the interaction of ambient flow with the divergence from convective cells (Heymsfield and Schotz 1985; Smull and Houze 1987).

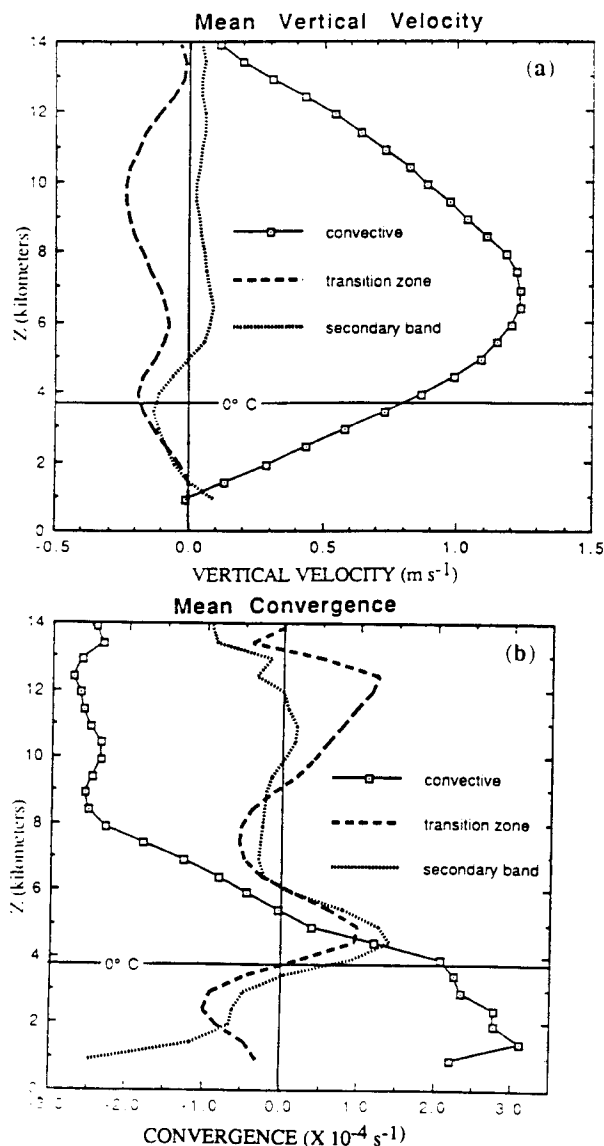


Fig. 4 Composite storm profiles of (a) vertical motion and (b) convergence in the convective region, transition zone, and the secondary band.

#### 4. UPPER-LEVEL CONVECTIVE DOWNDRAFTS

In the numerical simulation of Fovell and Ogura (1988), the region of subsidence behind the convective line was found to be the net result of weakening updrafts and expanding downdrafts associated with dissipating, transient convective cells which propagated rearward relative to the front edge of the storm. High resolution dual-Doppler analyses at individual times (e.g. Fig. 5) indicate that a similar process may have occurred in the observed storm, where an analogous series of convective updrafts and downdrafts were found. To understand how the mean subsidence in the upper-level transition zone downdraft may have developed, we used the near instantaneous three-dimensional individual dual-Doppler analyses to examine the structure of several vertical drafts found along the rear of the convective region. Each draft was tracked from upper levels to the lowest level at which a distinct maximum in downward motion could be found.

The profile of vertical velocities averaged over the area of each draft reveals a double peak similar to that

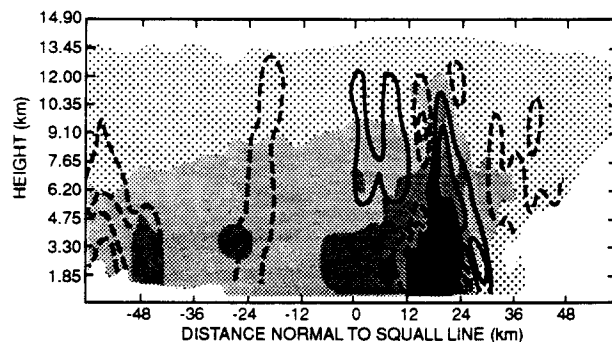


Fig. 5 Cross section of vertical velocity (dashed lines -6, -3, -1 m s<sup>-1</sup>; solid lines 3, 6 m s<sup>-1</sup>) and reflectivity (shaded every 5 dBZ starting at 5 dBZ) from the 0139 UTC dual-Doppler analysis.

observed for the mean subsidence in the transition zone (Fig. 6a). In each of the drafts examined along the rear of the convective region, the strongest averaged downdraft occurred at upper levels. An apparently separate peak was found near the melting level. The upper-level downdrafts were typically 2 to 3 m s<sup>-1</sup> on average, but had maximum values close to 5 m s<sup>-1</sup>. The strongest upper-level downdraft was close to 10 m s<sup>-1</sup>. As a result of the inherent resolution of the data (about a 6-km wavelength for the drafts examined) and the 6-km filter applied to the horizontal winds before computing divergence, the exact values of maxima are underestimated.

Profiles of convergence averaged over the area of the drafts indicate that the upper-level downdrafts were associated with very intense, but shallow, convergence near cloud top (Fig. 6b). The shallow forcing near cloud top suggests that the upper-level downdrafts may have been a manifestation of gravity waves excited by the interaction between the stable ambient air and strong convective updrafts. In each case, the downdraft was located to the rear of a strong convective updraft.

The areas covered by the downdrafts were typically greatest near storm top and decreased rapidly toward the ground before increasing slightly again near the melting level (Fig. 6c). Thus, the upper-level forcing produced a relatively shallow but strong response over a significant region to the rear of the convective updrafts.

#### 5. CONCLUSIONS

The mean downdraft in the transition zone of the 10-11 June 1985 squall line apparently consisted of two distinctly different types of downdraft. The upper-level downdraft, which was likely positively buoyant, was associated with a peak in convergence near storm top. The lower-level downdraft was associated with a separate peak in convergence just above the melting level and was likely affected by cooling from melting and evaporation.

The mean subsidence at upper levels in the transition zone was apparently the net result of transient vertical drafts associated with dissipating convective cells as they moved rearward relative to the front edge of the storm. Individual convective downdrafts along the back of the convective region exhibited a double peak in speed maxima similar to the mean subsidence in the transition zone. The strongest speed and greatest areal extent of the downdrafts were observed at upper levels in association with intense shallow layers of convergence to the rear of strongly diverging convective updrafts.

While a reflectivity trough at mid-to-low levels was associated with the deep subsidence in the transition zone, the cold temperatures at the high altitudes where the upper-level downdrafts were observed makes it unlikely that the upper-level downdrafts significantly reduced the mass of the falling hydrometeors. However, the lower-level peak in the

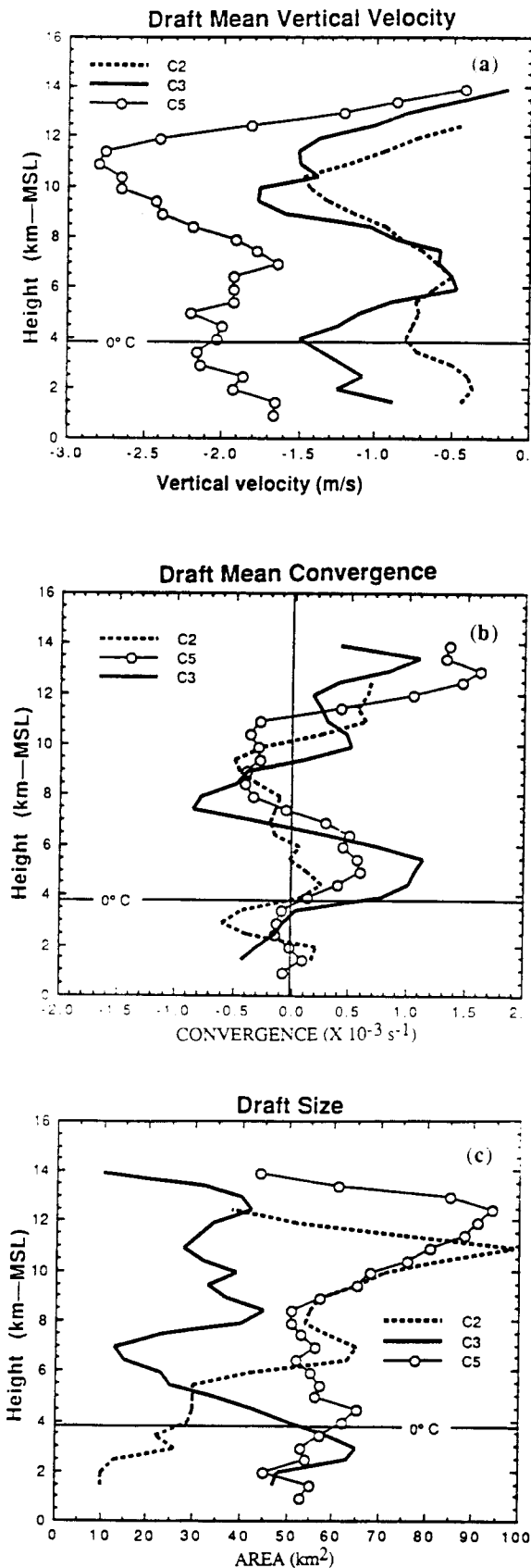


Fig. 6 Vertical profiles from three individual convective downdrafts along the back of the convective region showing (a) average vertical velocity, (b) average convergence, and (c) area covered.

subsidence was deep enough and at warm enough levels that the mass of the hydrometeors may have been significantly reduced through sublimation and evaporation as they fell toward the surface.

The role of the upper-level downdraft on the precipitation structure of the trailing-stratiform region may have been to aid indirectly in the development of the secondary precipitation maximum associated with an enhanced mesoscale updraft along the front edge of the secondary band. Since the upper-level transition-zone downdraft was positively buoyant, air flowing through it was dynamically forced to descend. Once the air was beyond the upper-level dynamic forcing associated with the convective- and transition-zone regions, it would have accelerated back to its equilibrium level, creating a region of enhanced upward motion.

#### ACKNOWLEDGEMENTS

Dr. D. Churchill and H. Terri transferred the Doppler-radar analysis software from NCAR to the University of Washington. S. Braun and M.-J. Yang digitized the relative flow fields. G. Gudmundson edited the manuscript and K. Dewar drafted the figures. This research was funded by the National Science Foundation under grant ATM-8719838.

#### REFERENCES

- Biggerstaff, M.I., and R.A. Houze, Jr., 1991: Comprehensive analysis of the 10-11 June 1985 PRE-STORM squall line. Part I: Precipitation and kinematic structure. Conditionally accepted *Mon. Wea. Rev.*
- Cunning, J.B., 1986: The Oklahoma-Kansas preliminary regional experiment for STORM-Central. *Bull. Amer. Meteor. Soc.*, **67**, 1478-1486.
- Fovell, R.G., and Y. Ogura, 1988: Numerical simulation of a midlatitude squall line in two dimensions. *J. Atmos. Sci.*, **45**, 3846-3879.
- Heymsfield, G.M., and S. Schotz, 1985: Structure and evolution of a severe squall line over Oklahoma. *Mon. Wea. Rev.*, **113**, 1563-1589.
- Houze, R.A., Jr., S.A. Rutledge, M.I. Biggerstaff and B.F. Smull, 1989: Interpretation of Doppler weather-radar displays of midlatitude mesoscale convective systems. *Bull. Amer. Meteor. Soc.*, **70**, 608-619.
- Johnson, R.H., and P.J. Hamilton, 1988: The relationship of surface pressure features to the precipitation and air flow structure of an intense midlatitude squall line. *Mon. Wea. Rev.*, **116**, 1444-1472.
- Rutledge, S.A., R.A. Houze, Jr., M.I. Biggerstaff and T. Matejka, 1988: The Oklahoma-Kansas mesoscale convective system of 10-11 June 1985: Precipitation structure and single-Doppler radar analysis. *Mon. Wea. Rev.*, **116**, 1409-1430.
- Smull, B.F., and R.A. Houze, Jr., 1987: Dual-Doppler radar analysis of a midlatitude squall line with a trailing region of stratiform rain. *J. Atmos. Sci.*, **44**, 2128-2148.
- Sun, J., R.A. Houze, Jr., R.G. Fovell and M.I. Biggerstaff, 1991: Thermodynamic structure of the trailing-stratiform region of a squall line. Submitted to *Mon. Wea. Rev.*